Generation of tumorigenic porcine pancreatic ductal epithelial cells: toward a large animal model of pancreatic cancer

Neeley Remmers[1,2], Jesse L. Cox[3], James A. Grunkemeyer[4], Shruthi Aravind[1,2], Christopher K. Arkfeld[1,2], Michael A. Hollingsworth[4], Mark A. Carlson[1,2,5*]

[1]Department of Surgery, University of Nebraska Medical Center, Omaha, NE, USA

[2] Surgery Department, VA Nebraska-Western Iowa Health Care System, Omaha, NE, USA

[3]Department of Pathology and Microbiology, University of Nebraska Medical Center, Omaha, NE, USA

[4]Eppley Cancer Institute, University of Nebraska Medical Center, Omaha, NE, USA

[5]Department of Genetics, Cell Biology and Anatomy, University of Nebraska Medical Center, Omaha, NE, USA

*Corresponding author

Email: macarlso@unmc.edu (MAC)

Abstract

Background. A large animal model of pancreatic cancer would permit development of diagnostic and interventional technologies not possible in murine models, and also would provide a more biologically-relevant platform for penultimate testing of novel therapies, prior to human testing. Here, we describe our initial studies in the development of an autochthonous, genetically-defined, large animal model of pancreatic cancer, using immunocompetent pigs.

Methods. Primary pancreatic epithelial cells were isolated from pancreatic duct of domestic pigs; epithelial origin was confirmed with immunohistochemistry. Three transformed cell lines subsequently were generated from these primary cells using expression of oncogenic KRAS and dominant negative p53, with/without knockdown of p16 and SMAD4. We tested these cell lines using *in vitro* and *in vivo* assays of transformation and tumorigenesis.

Results. The transformed cell lines outperformed the primary cells in terms proliferation, population doubling time, soft agar growth, 2D migration, and Matrigel invasion, with the greatest differences observed when all four genes (KRAS, p53, p16, and SMAD4) were targeted. All three transformed cell lines grew tumors when injected subcutaneously in nude mice, demonstrating undifferentiated morphology, mild desmoplasia, and staining for both epithelial and mesenchymal markers. Injection into the pancreas of nude mice resulted in distant metastases, particularly when all four genes were targeted.

Conclusions. Tumorigenic porcine pancreatic cell lines were generated. Inclusion of four genetic "hits" (KRAS, p53, p16, and SMAD4) appeared to produce the best results in our *in vitro* and *in vivo* assays. The next step will be to perform autologous or syngeneic implantation of these cell lines into the pancreas of immunocompetent pigs. We believe that the resultant large animal model of pancreatic cancer could supplement existing murine models, thus improving preclinical research on diagnostic, interventional, and therapeutic technologies.

52 # Introduction

53 In the United States in 2016, approximately 53,000 people (48% female) were diagnosed
54 with pancreatic cancer (~3.1% of all new cancer diagnoses), and there were ~42,000 deaths (49%
55 female) from pancreatic cancer (~7.0% of all cancer deaths) [*1, 2*]. The lifetime risk for
56 pancreatic cancer is approximately 1 in 65 [*1, 2*]. The incidence of pancreatic cancer has been
57 gradually increasing since the mid-1990's, and generally is higher in the African-American
58 population [*1, 2*]. Pancreatic cancer is now is the fourth most common cause of cancer-related
59 death in both men and women (after lung, prostate, and colorectal cancer, or lung, breast, and
60 colorectal cancer, respectively) [*1, 2*]. Despite apparent advances in treatment modalities and
61 strategies [*3, 4*], mortality from pancreatic cancer has not decreased [*1, 2*]. As of 2012, the U.S.
62 overall 5-year survival rate from pancreatic cancer was 7.7%; 5-year survival rates in localized,
63 regional (nodal spread), or metastatic disease were 29.3, 11.1, and 2.6%, respectively [*1, 2*]. So
64 there remains a need for improved early diagnosis and therapy for pancreatic cancer.

65 Rodent models of pancreatic cancer may not accurately reflect human biology because of
66 differences in physiology, anatomy, immune response, and genetic sequence between the two
67 species [*5-8*]. Remarkably, only 5-8% of anti-cancer drugs that emerged from preclinical studies
68 and entered clinical studies have been ultimately approved for clinical use [*9, 10*]. The cause of
69 this low approval rate is multifactorial, but likely includes the less-than-optimal predictive ability
70 of some murine models (e.g., tumor xenografting into immunosuppressed mice) to determine the
71 efficacy of various therapeutics in humans [*5-7, 11-15*]. Moreover, there are a number of genes
72 for which the genotype-phenotype relationship is discordant between mice and human, including
73 *CFTR*$^{-/-}$ and *APC*$^{+/-}$ [*16, 17*]. Incidentally, both the porcine *CFTR*$^{-/-}$ and *APC*$^{+/-}$ mutants reiterate

74 the human phenotype (pulmonary/GI disease and rectal polyposis, respectively) [*16-18*], in
75 contradistinction to the murine mutants.
76 In fairness, the recent trend to employ genetically-engineered mouse models (GEMM),
77 patient-derived xenografts (PDX), humanized mice, and *in vivo* site-directed CRISPR/Cas9
78 gene-edited mice in the testing of anti-cancer therapeutics may yield murine models with better
79 predictive ability than obtained with previously [*7, 19-23*]. Though promising, these more
80 advanced murine models come with increased cost and complexity [*21*], and experience with
81 them still is early. Importantly, all murine models have limited utility in the development of
82 diagnostic or interventional technology that requires an animal subject whose size approximates
83 a human. So at present, there remains a need for improved animal models of pancreatic cancer
84 that (1) are more predictive of human response to anti-cancer therapy [*21, 23*], and (2) are of
85 adequate size for development of specific technologies. Herein we describe some initial steps
86 taken in the development of a genetically-defined, autochthonous model of pancreatic cancer in
87 immunocompetent pigs.
88

Materials and Methods

Standards, rigor, reproducibility, and transparency

The animal studies of this report were designed, performed, and reported in accordance with both the ARRIVE recommendations (Animal Research: Reporting of *In Vivo* Experiments [*24*]) and the National Institutes of Health Principles and Guidelines for Reporting Preclinical Research [*25, 26*]; for details, refer to Tables S1 and S2, respectively.

Materials and animal subjects

All reagents were purchased through Thermo Fisher Scientific (www.thermofisher.com) unless otherwise noted. Short DNA sequences for vector construction, mutagenesis, and amplification purposes are shown in Table S3. Antibody information is given in Table S4. Wild type domestic swine (male and female; age 3 months at time of purchase; 30-32 kg) were purchased from the Animal Research and Development Center of the University of Nebraska Lincoln (ardc.unl.edu). Athymic homozygous nude mice (Crl:NU(NCr)-*Foxn1*^{nu}; female; 8-9 weeks old) were purchased from Charles River Laboratories, Inc. (www.criver.com). Primers utilized in this report (Table S3) were synthesized by Integrated DNA Technologies, Inc. (www.idtdna.com). DNA sequencing was performed by the UNMC Genomics Core Facility (www.unmc.edu/vcr/cores/vcr-cores/genomics).

Animal welfare

110 The animals utilized to generate data for this report were maintained and treated in
111 accordance with the *Guide for the Care and Use of Laboratory Animals* (8th ed.) from the
112 National Research Council and the National Institutes of Health [*27*], and also in accordance
113 with the Animal Welfare Act of the United States (U.S. Code 7, Sections 2131 – 2159). The
114 animal protocols pertaining to this manuscript were approved by the Institutional Animal Care
115 and Use Committee (IACUC) of the VA Nebraska-Western Iowa Health Care System (ID
116 numbers 00927, 00937, 00998, and 01017) or by the IACUC of the University of Nebraska
117 Medical Center (ID number 16-133-11-FC). All procedures were performed in animal facilities
118 approved by the Association for Assessment and Accreditation of Laboratory Animal Care
119 International (AAALAC; www.aaalac.org) and by the Office of Laboratory Animal Welfare of
120 the Public Health Service (grants.nih.gov/grants/olaw/olaw.htm). All surgical procedures were
121 performed under isoflurane anesthesia, and all efforts were made to minimize suffering.
122 Euthanasia was performed in accordance with the AVMA Guidelines for the Euthanasia of
123 Animals [*28*].
124

125 Isolation of porcine pancreatic ductal epithelial cells

126 A detailed protocol for isolation of porcine pancreatic ductal epithelial cells is provided
127 in the Supporting Information. In brief, the intact pancreas from male porcine research subjects
128 (age 5 mo) was harvested within 5 min after euthanasia, which was accomplished by transection
129 of the intrathoracic inferior vena cava and exsanguination while under deep isoflurane
130 anesthesia. These pigs had been on a protocol to study biomaterials within skin wounds of the
131 dorsum. The subject had not received any recent medication other the anesthetics given for
132 euthanasia; buprenorphine and cefovecin sodium had been given 4 weeks prior to euthanasia.

133 Immediately after explantation of the pancreas, the main pancreatic duct was dissected sterilely
134 with micro instruments from the organ body under 3.5x loupe magnification. The duct then was
135 mechanically digested by passage through a 70 µm sieve (Corning™ Sterile Cell Strainers,
136 Thermo Fisher Scientific, cat. no. 07-201-431).

137 The collected fragments were enzymatically digested with 1 mg/mL of Collagenase D at
138 37˚C for 1 h with gentle shaking. The cells were pelleted (600 *g* x 5 min), the supernatant was
139 discarded, the cell pellet was resuspended in whole media, which was defined as: DMEM (high
140 glucose with L-glutamine; Thermo Fisher Scientific, cat. no. 12100-046) supplemented with
141 10% (final concentration) fetal bovine serum (FBS; Thermo Fisher Scientific, cat. no. 26140079)
142 and 1% Antibiotic-Antimycotic Solution (Corning Inc., cat. no. 30-004-CI; cellgro.com). Cell
143 concentration in the resuspension was determined with a hemocytometer, and cells then were
144 diluted and pipetted into a 96-well plate (1-10 cell/well, 100-200 µL/well). After 5-7 days of
145 culture under standard conditions (whole media, 37˚C, 5% CO_2), wells that contained cells with
146 epithelial-like morphology were trypsinized and re-plated into a new 96-well plate, in order to
147 dilute out any fibroblasts. Cells were passaged in this fashion at least four times, until no cells
148 with fibroblast morphology were present. The resulting cells were passaged up to a T25 flask,
149 and maintained with standard conditions.

150

151 Generation of p53 and KRAS mutants and construction of
152 expression vector

153 In order to generate the porcine $p53^{R167H}$ mutant, wild-type p53 cDNA first was amplified
154 from cervical lymph node tissue, which was obtained <5 min after euthanasia of a 4 month old
155 male domestic swine that had been on an unrelated research protocol. In brief, fresh nodal tissue

156 was flash-frozen in liquid N_2 and then pulverized with a mortar and pestle, with continual
157 addition of liquid N_2 during pulverization. The frozen powder then was placed into the first
158 buffer solution of the QIAGEN RNEasy Mini Kit (cat. no. 74104; www.qiagen.com), and total
159 RNA was isolated per the manufacturer's instructions.

160 After isolation, the total RNA underwent reverse transcription to cDNA with a Verso
161 cDNA Synthesis Kit (Thermo Fisher Scientific, cat. no. AB1453A), per the manufacturer's
162 instructions. The wild type p53 sequence was amplified out of the cDNA using the PCR primers
163 shown in Table S3, which flanked the p53 cDNA with *Sal*I and *Bam*HI restriction sites.
164 Successful amplification of the wild-type p53 cDNA was confirmed by inserting the amplified
165 candidate sequence into the TOPO® vector (TOPO® TA Cloning® Kit; Invitrogen™/Life
166 Technologies™, Thermo Fisher Scientific, cat. no. K202020) per the manufacturer's
167 instructions, followed by sequencing.

168 Site-directed mutation of wild-type p53 into $p53^{R167H}$ was performed using Agilent
169 Technologies' QuickChange II Site-Directed Mutagenesis Kit (cat. no. 200523;
170 www.genomics.agilent.com) with the mutagenic primers shown in Table S3, per the
171 manufacturer's instructions. Presence of the $p53^{R167H}$ mutation was verified by sequencing as
172 described above. The multiple cloning site of a pIRES2-AcGFP1 Vector (Takara Bio USA, Inc.,
173 cat. no. 632435; www.clontech.com; manufacturer's vector information included as **Fig. S1**) was
174 cut with *Sal*I and *Bam*HI, and the $p53^{R167H}$ sequence then was ligated into this plasmid.

175 The source of the porcine $KRAS^{G12D}$ mutant was the plasmid used to generate the
176 p53/KRAS Onco-pig [*29, 30*]. The $KRAS^{G12D}$ cDNA was amplified out of this plasmid with
177 primers (see Table S3) that flanked the sequence with *Xho*I and *Pst*I restriction sites. The
178 amplified product was inserted into the TOPO vector and verified by sequencing, as described

179 above. The above pIRES2-AcGFP1 Vector (already containing the $p53^{R167H}$ sequence) then was
180 cut with *Xho*I and *Pst*I, and the $KRAS^{G12D}$ sequence was ligated into this plasmid, producing a
181 pIRES2-AcGFP1 Vector which contained both mutant cDNAs within its multiple cloning site
182 ($KRAS^{G12D}$ upstream).

183 The newly-constructed plasmid, hereafter designated as GKP (G = AcGFP1; K =
184 $KRAS^{G12D}$; P = $p53^{R167H}$), was transformed into One Shot™ Stbl3™ Chemically Competent *E.*
185 *coli* (Invitrogen™/Thermo Fisher Scientific, cat. no. C737303), per the manufacturer's
186 instructions, and plasmid DNA subsequently was isolated using a QIAGEN Plasmid Maxi Kit
187 (cat. no. 12162), per the manufacturer's instructions. This plasmid then was transfected into
188 Takara's Lenti-X™ 293T cells (Clontech, cat. no. 632180), using Takara's Xfect™ Transfection
189 Reagent (Clontech, cat. no. 631317), per the manufacturer's instructions, to generate infectious
190 lentiviral particles that would direct expression of AcGFP1, $KRAS^{G12D}$, and $p53^{R167H}$ mutants in
191 transduced cells.

192

193 # Generation of shRNA-expressing vectors

194 Short hairpin RNA (shRNA) constructs targeting the porcine SMAD4 and p16 genes
195 were created using InvivoGen's siRNA Wizard™ software (www.invivogen.com/sirnawizard).
196 Three targeting sequences for each gene along with scrambled controls initially were generated
197 and tested. The shRNA construct that demonstrated the best target knock-down in preliminary
198 experimentation (as verified by PCR, data not shown) was utilized for subsequent experiments
199 (see Table S3 for sequences ultimately selected for the shRNA constructs). Primers were cloned
200 into the psiRNA-h7SKhygro G1 and psiRNA-h7SKneo G1 vectors (InvivoGen, cat. no. ksirna3-

201 h21 and ksirna3-n21, respectively; www.invivogen.com) and plasmids then were isolated, all per
202 the manufacturer's protocol.
203

204 Cell transformations

205 Primary porcine pancreatic epithelial cells in T75 flasks were grown to 80% confluency
206 under standard conditions. The media then was exchanged with 2-3 mL of supernatant from non-
207 lysed Lenti-X™ 293T cells (containing GKP viral particles) with 2 µg/mL polybrene (cat. no.
208 TR1003, Thermo Fisher Scientific). After 24-48 h at 37˚C, treated epithelial cells were re-seeded
209 into 6-well plates under standard conditions and grown to 80% confluency. An exchange with
210 whole media containing 2 µg/mL G418 aminoglycoside antibiotic then was performed; the G418
211 dose was chosen based on preliminary dose-response studies against non-treated epithelial cells.
212 After 24 h, a whole media exchange was done, and the presence of transduced cells was
213 determined with inverted GFP fluorescent microscopy of living cells. Subsequent transfections
214 for RNAi were done with the above plasmids employing shRNA sequences against SMAD4
215 and/or p16, and using the LyoVec™ reagent (InvivoGen, cat. no. lyec-12), all per the
216 manufacturer's protocol. Transfected cells then were selected for expression of the shRNA
217 vector using the appropriate aminoglycoside antibiotic (G418 or hygromycin B).
218

219 PCR

220 Cell and tissue RNA was isolated using the QIAGEN RNEasy Mini Kit. Purified RNA
221 then was used to generate cDNA using the Verso cDNA Synthesis Kit. The Platinum® Blue
222 PCR Supermix (Invitrogen™/Life Technologies, cat. no. 12580) subsequently was used for all
223 PCR reactions. Amplified products were separated with agarose gel electrophoresis, and then

224 visualized using a UV-light box. qPCR was performed using the PowerUp™ SYBR® Green
225 Master Mix (Applied Biosystems™/ Thermo Fisher Scientific, cat. no. A25741) per
226 manufacturer's protocol, and run on an Applied Biosystems™ 7500 Fast Dx Real-Time PCR
227 Instrument. Fold changes in gene expression were calculated using the comparative C_T method
228 [*31*]. All primers used are listed in Table S3.
229

230 # Immunoblotting

231 Western blot analysis was performed to confirm overexpression of the mutant p53 protein
232 (see Table S4 for a list of antibodies used), as previously described [*32*]. An antibody specific for
233 the mutant KRAS protein was not commercially available. Antibody expression was visualized
234 using the Li-Cor Odyssey Electrophoresis Imaging System (www.licor.com).
235

236 # Soft agar assay

237 A standard soft agar assay [*33*] was used to determine anchorage independent growth. A
238 base layer of 1% agarose was plated into 6-well plates. A total of 2,500 cells/well were mixed
239 with 0.7% agarose and plated on top of the base layer. The plates were incubated under standard
240 conditions for 21 days. The cells then were stained with crystal violet, and counted using an
241 inverted microscope. Cells were plated in triplicate, and total counts from all three wells were
242 averaged.
243

244 # Migration assay

245 A standard scratch assay (monolayer wounding) [*34*] was performed to determine cellular
246 migration rate. Cells were plated in triplicate into 6-well plates. A horizontal scratch using a 10
247 μL pipet tip was made in each well. After washing away scratched-off cells, baseline images
248 along the scratch were obtained, the plates were incubated under standard conditions, and
249 subsequent images were captured at 3, 6, 9, 12, and 15 h after the initial scratch. ImageJ software
250 (imagej.nih.gov/ij) was used to measure the distance between the two migrating cellular fronts
251 (scratch edges) at 3-5 locations along the scratch. Average distance at each time point was
252 plotted to generate the migratory rate (μm/h).
253

254 # Invasion assay

255 BioCoat™ Matrigel™ Invasion Chambers (Corning™, Thermo Fisher Scientific, cat. no.
256 08-774) were plated with 50,000 cells (upper chamber) in triplicate, and incubated under
257 standard conditions for 24 h. The media from the upper chamber then was removed, and any
258 cells remaining in the upper chamber were removed using a cotton swab. Cells that had migrated
259 to the bottom of the membrane were stained using a Kwik-Diff™ kit (Shandon™, Thermo Fisher
260 Scientific, cat. no. 9990701). Membranes were mounted onto glass slides, and cells per high-
261 power field were counted using ImageJ software.
262

263 # Population doubling assay

264 Cells were plated in 6-well plates (20,000 cell/well), and cultured under standard
265 conditions. Triplicate plates then were trypsinized on days 1, 2, 3, 4, 6, and 8, and cells were
266 counted with a hemocytometer. Cell number *vs*. day was plotted to determine the day range in
267 which linear growth was achieved. The data from this linear growth phase were used to

268 determine population doubling time (DT) using the formula: $DT = (\Delta t) \times \ln(2) \div \ln(N_f/N_i)$
269 where Δt = time interval between initial and final cell count, N_f = cell count at final time, and N_i
270 = cell count at initial time.
271

272 # Proliferation assay

273 Relative cell proliferation rates were assayed using an MTT (3-(4,5-dimethylthiazol-2-
274 yl)-2,5-diphenyltetrazolium bromide) assay kit (Vybrant™ MTT Cell Proliferation Assay Kit,
275 Invitrogen™, Thermo Fisher Scientific, cat. no. V13154). Cells were plated in triplicate in a 96-
276 well plate (5,000 cell/well), and cultured under standard conditions for 48 h. MTT reagent then
277 was added to the cells per the manufacturer's instructions, followed by addition of the solvent
278 solution 3.5 h later. Absorbance was measured with a plate reader 3.5 h after solvent addition.
279 Mean absorbance was normalized to absorbance from wild type pancreatic ductal epithelial cells
280 to calculate fold-difference in proliferation.
281

282 # Immunofluorescence and immunohistochemistry

283 Antibodies used in immunofluorescent and immunohistochemical experiments are listed
284 in Table S4. Agilent Dako EnVision kits (www.agilent.com) were used for all IHC analyses per
285 the manufacturer's instructions.
286

287 # Subcutaneous tumorigenic cell injection

288 Subcutaneous implantation of tumorigenic cells was performed as previously described
289 [*35*], with some modifications. Tumorigenic porcine pancreatic ductal epithelial cells were

290 trypsinized, counted, and resuspended in DMEM at a concentration of 1×10^7 viable cells/mL.
291 Nude mice (N = 10 per treatment group) then were injected with 5×10^6 cells (500 μL) into the
292 right hind flank. Tumors were allowed to grow for 6 weeks or until they reached 1.8 cm in
293 diameter, as measured with a caliper. At necropsy all gross tumor was measured and collected,
294 portions underwent formalin fixation and paraffin embedding, and sections subsequently
295 underwent H&E or immunohistochemical staining as described above. An independent, blinded
296 pathologist analyzed the stained sections to determine whether tumors were epithelial in origin,
297 and if they displayed malignant features.
298

299 # Orthotopic tumorigenic cell injection

300 Orthotopic implantation of tumorigenic cells was performed as previously described [*35*]
301 to analyze metastases and desmoplasia. In brief, tumorigenic porcine pancreatic ductal epithelial
302 cells were trypsinized and counted, and 1×10^4 viable cells in 20 μL DMEM were injected with
303 a 20 gauge needle into the pancreas of nude mice (N = 10-12 per treatment group) through a 5
304 mm incision in the left upper quadrant. Mice were euthanized 6 weeks after injection, and tumors
305 and organs were harvested for gross and histologic analysis, as described in the previous
306 paragraph.
307

308 # Statistical analysis

309 Data are reported as mean ± standard deviation. Groups of continuous data were
310 compared with ANOVA and the unpaired t-test.
311
312

313 # Results

314

315 ## Isolation of primary porcine pancreatic ductal epithelial cells

316 Cells cultured from micro-dissected pancreatic ducts displayed epithelial morphology
317 under phase microscopy and stained for CK19 (an established marker of pancreatic ductal
318 epithelium [*36*]; **Fig. 1A-B**). Based on these results, we were confident that we had a population
319 of pancreatic epithelial cells that we could use to generate tumorigenic cell lines.

320

321 ## Generation of tumorigenic cell lines

322 In order to transform our primary porcine pancreatic ductal epithelial cells, we first
323 generated a lentiviral construct containing *KRAS*^{G12D} and *TP53*^{R167H}, genes previously identified
324 [*29*] as the porcine equivalents to the mutant *KRAS* and *TP53* which are present in multiple
325 human cancers [*37-41*]; in the mouse, expression of these mutants was the basis for the
326 KRAS/p53 genetically engineered murine model of pancreatic cancer [*42*]. For our model, we
327 chose to use a lentiviral platform for the vector, because its genome would be large enough to
328 accommodate insertion of both mutant genes; in addition, we believed that a lentivirus would be
329 optimal for transforming primary cells.

330 Since initial sequencing of the porcine genome has been accomplished [*43*], we were able
331 to utilize the National Library of Medicine's nucleotide BLAST® database
332 (blast.ncbi.nlm.nih.gov/blast.cgi) to determine the porcine genetic equivalents for human *SMAD4*
333 and *CDKN2A*. We then designed primers (Table S3) to amplify these two genes from genomic
334 DNA isolated from skin of a healthy domestic pig. We sequenced our amplification products,

335 and accessed the BLAST® database to confirm that our products aligned with the porcine
336 *SMAD4* and *CDKN2A* gene sequences. We then proceeded to generate lentiviral constructs to
337 transform primary porcine pancreatic ductal epithelial cells into cell lines expressing various
338 combinations of mutant KRAS and p53, SMAD4 shRNA, and $p16^{Ink4A}$ shRNA (see cell line
339 definitions in Table 1), as described under Materials and Methods.

340 Primary porcine epithelial cells next were transduced with the GKP lentivirus to generate
341 transformed cell lines. Overexpression of $KRAS^{G12D}$ and $p53^{R167H}$ was confirmed in these cell
342 lines with qPCR and immunoblotting (**Fig. 1C-E**). Of note, we could not obtain a reliable
343 antibody to detect porcine KRAS with immunoblotting, so we had to rely on qPCR results and
344 expression of GFP as markers of $KRAS^{G12D}$ expression. Preliminary *in vitro* analyses to probe
345 the tumorigenic properties of these GKP-transformed cell lines demonstrated modest increases in
346 soft agar colony formation and migration speed over wild type cells (**Fig. 2A & B**). Interestingly,
347 the cell line (2.22) with the best performance in the soft agar and migration assays had only
348 modest overexpression of $KRAS^{G12D}$ and $p53^{R167H}$ (**Fig. 1 & 2**); in contrast, the cell lines with
349 the highest mutant overexpression performed relatively poorly in these *in vitro* assays of
350 "tumorigenesis" (i.e., evidence of transformed behavior in cell culture).

351 While *in vitro* experiments were being performed, *in vivo* pancreatic tumor induction was
352 attempted utilizing a transgenic mini-pig available from the National Swine Resource and
353 Research Center (NSRRC; nsrrc.missouri.edu). Known as the "Onco-pig," [*30*], this subject
354 carries an LSL-cassette containing the dominant negative $TP53^{R167H}$ and the activated $KRAS^{G12D}$
355 sequences [*30, 44, 45*]; i.e., this subject is the porcine analog of the KRAS/p53 mouse [*42, 46*].
356 As demonstrated previously, site-specific expression of Cre recombinase in the Onco-pig
357 resulted in localized p53 inhibition and KRAS activation, while subcutaneous injection of AdCre

358 produced mesenchymal tumors at the injection sites [*30*]. We injected Cre recombinase into the
359 pancreas of five Onco-pigs (**Fig. S2**). After four months, we observed no gross tumors. However,
360 there was immunohistochemical evidence of transgene expression at the pancreatic injection
361 sites along with numerous microscopic proliferative lesions (**Fig. S2**).

362 Based on the modest evidence of *in vitro* transformation and the lack of gross *in vivo*
363 tumorigenesis using expression of $p53^{R167H}$ and $KRAS^{G12D}$ only, we decided that additional
364 oncogenic stress might be helpful to increase the tumor-like properties of transformed pancreatic
365 ductal epithelial cells. Utilizing cell line 2.22 (hereafter referred to PGKP; see Table 1), which
366 had relatively good performance in the soft agar and migration assays (**Fig. 2A & B**), sequential
367 transduction with lentiviral constructs expressing shRNA against SMAD4 and then $p16^{Ink4A}$ was
368 performed to generate cell lines PGKPS and PGKPSC (see Table 1), respectively. RT-PCR then
369 was used to confirm knockdown of the targeted transcripts in these two cell lines (**Fig. 2C**).
370

371 ## *In vitro* tumorigenic properties of transformed cells

372 The *in vitro* "tumorigenic" properties of the PGKP, PGKPS, and PGKPSC cell lines first
373 were compared with the soft agar and migration assays (**Fig. 2D & E**). Addition of SMAD4 ±
374 $p16^{Ink4A}$ knockdown enhanced the ability of transformed cells to form colonies in soft agar and
375 increased their migration speed (2D wounding assay), particularly when both transcripts were
376 targeted (i.e., the PGKPSC line). We then compared population doubling time, proliferation
377 (metabolic dye conversion) , and Matrigel® invasion ability among the three transformed lines
378 with respect to wild type cells (**Fig. 3A-C**). Both the PGKPS and PGKPSC cell lines had greater
379 proliferation and invasive ability compared to either wild type cells or the PGKP cell line (**Fig.
380 3B, C**). The doubling time for all three transformed cell lines was approximately the same at ~15

381 h, compared to the ~4 d doubling time of wild type cells (**Fig. 3A**). Based on the *in vitro* assays
382 of tumorigenesis, we suspected that all three of our transformed cell lines had the potential to
383 form tumors *in vivo*, albeit to varying degrees. We subsequently decided to compare the *in vivo*
384 tumorigenicity among all three cell lines in an immunodeficient mouse model.
385

386 Subcutaneous and orthotopic tumor transplants in immunodeficient 387 mice

388 In order to determine if our cell lines retained their tumorigenic properties *in vivo*, we
389 utilized homozygous athymic mice to generate subcutaneous and orthotopic cell implantation
390 models. The subcutaneous model was used to assess *in vivo* tumor growth. All three cell lines
391 grew sizeable tumors (>1 cm diameter) within 6 weeks; growth rates were not statistically
392 different among the three cell lines (**Fig. 4A & B**). The subcutaneous tumors were well-
393 vascularized and mucinous in gross appearance (**Fig. 4A**). Confirmation of GKP lentiviral
394 transduction was demonstrated with immunohistochemistry of the $p53^{R167H}$ mutant in
395 subcutaneous tumors (**Fig. S3**).
396 Tumors from the subcutaneous implant model then underwent immunohistochemical
397 staining with an array of epithelial and mesenchymal markers (**Fig. 5**). The distribution of
398 staining for the epithelial markers (E-cadherin, epithelial cell adhesion molecule, pan-
399 cytokeratin, cytokeratin-19) generally was more diffuse than the mesenchymal marker staining.
400 In some regions the epithelial marker staining was clustered and intense. The overall abundance
401 of staining for the epithelial markers appeared greater in the PGKPS and PGKPSC lines with
402 respect to the PGKP line. The distribution of staining for the mesenchymal markers (α-smooth
403 muscle actin, vimentin, and type I collagen) was variable, sometimes appearing in cords or

404 strands in some sections, reminiscent of the desmoplastic reaction in human pancreatic cancer
405 [*47, 48*]. In other sections, mesenchymal marker staining was minimal. Similar to the epithelial
406 markers, the overall abundance of staining for the mesenchymal markers appeared greater in the
407 PGKPS and PGKPSC lines compared to the PGKP line.

408 With the immunohistochemical studies of the subcutaneous tumors demonstrating some
409 epithelial characteristics, the nude mouse orthotopic implantation model was used next to assess
410 the metastatic potential of all three cell lines. The percentage of mice implanted with each cell
411 line that subsequently developed metastasis in the small bowel, diaphragm, liver, lung, lymph
412 node, peritoneum, or spleen is shown in **Fig. 4C.** The degree of metastatic spread was minimal;
413 nodal tissue was the only metastatic site common to all three lines. The PGKPCS cell line
414 exhibited the greatest array of metastatic spread, with the most common site being the spleen
415 (though it was not clear in two of five mice with splenic disease after PGKPSC implantation
416 whether the spleen was involved with extension from the primary tumor, or from direct seeding,
417 or whether these were true metastases). Interestingly, one of the two subjects with liver
418 metastasis after PGKPSC implantation had primary tumor within the gallbladder, rather than
419 within the pancreas. Similar to the subcutaneous tumor model, most tumors in the orthotopic
420 model were well-vascularized and mucinous in gross appearance.
421
422

423
424 # Discussion

425

426 Our overall goal with this project was to generate tumorigenic pancreatic cell lines that
427 could be used in an immunocompetent porcine model of pancreatic cancer. Current murine
428 models for pancreatic cancer will continue to be helpful, particularly for the study of molecular
429 mechanisms. However, murine models are limited in their ability to replicate human biology and
430 size, so a large animal model of pancreatic cancer likely would enhance our ability to develop
431 and test new diagnostic and treatment modalities for this disease. The data presented herein
432 demonstrated that wild type porcine pancreatic ductal epithelium can be transformed with
433 modulation of common tumor-associated target genes, and that these transformed cells
434 subsequently can grow tumors in immunodeficient mice. These data provide a pathway for the
435 construction of an autochthonous porcine model of pancreatic cancer, namely, orthotopic
436 implantation of tumorigenic pancreatic cells.

437 The rationale to build a porcine model of pancreatic cancer is (1) to have a platform for
438 diagnostic/therapeutic device development otherwise not achievable in murine models; and (2) to
439 have a highly predictive preclinical model in which anti-cancer therapies (including
440 immunotherapies) could be vetted/optimized prior to a clinical trial. Porcine biomedical models
441 have been used for decades in the fields of trauma and hemostasis [*49*], xenotransplantation [*50*],
442 dermal healing [*51*], toxicology [*52*], atherosclerosis [*53*], and cardiac regeneration [*54*], to name
443 a few. The rationale to use the pig in this modeling effort is that this species mimics human
444 genomics [*55-59*], epigenetics [*60*], physiology [*52, 55, 61, 62*], metabolism [*55, 62, 63*],
445 inflammation and immune response [*59, 64-68*], and size [*62, 69*] remarkably well (in particular,

446 better than mice), with reasonable compromises towards cost and husbandry [*62*]. Recently, a
447 porcine genome map was generated [*43*], and further coverage, annotation, and confirmation is
448 ongoing [*57*]. Genetic manipulation of pigs (including knockouts, tissue-specific transgenics,
449 inducible expression [*29, 70-77*]) with similar tools as used in the mouse is becoming more
450 routine, with new gene-edited porcine models emerging in 2015-2017 for diseases such as
451 atherosclerosis, cystic fibrosis, Duchenne muscular dystrophy, and ataxia telangiectasia [*45, 78*].
452 So based on the pig's relatively large size and its proven track record in replicating human
453 biology which, incidentally, is a demonstrably better replication than can be obtained with
454 rodents, we selected swine as the model organism for this pancreatic cancer project.

455 Commonly mutated genes in pancreatic cancer include *KRAS* [*79, 80*], *TP53* [*80-82*],
456 *SMAD4* [*80, 83*], and *CDKN2A* [*80, 84*]. Somatic activation of KRAS via the G12D mutation
457 ($KRAS^{G12D}$) in mice produced widely metastatic pancreatic tumors; survival duration in these
458 subjects decreased further with p53 inactivation [*42*]. Deletion of *SMAD4* or *CDKN2A* enhanced
459 tumor growth in a $KRAS^{G12D}$ murine pancreatic cancer model [*85, 86*]. Based on this published
460 data, we elected to induce porcine pancreatic tumors with targeting of *KRAS*, *TP53*, *SMAD4*, and
461 *CDKN2A*, through site-directed expression of mutant genes and shRNA targeting. In the future,
462 we will gene edit cell lines using the CRISPR/Cas9 system (as opposed to shRNA expression) to
463 effect specific gene deletions.

464 Research on immunocompetent large animal cancer models [*87*] includes prostate cancer,
465 for which there is a canine model [*88*]. A group in Munich has engineered (i) an *APC* mutant pig
466 that develops rectal polyposis [*17*] and (ii) a pig with Cre-inducible p53 deficiency [*75*]. In
467 addition, a group in Denmark has engineered a *BRCA* mutant pig [*89*]. In 2012 the NSRRC
468 (National Swine Resource and Research Center, nsrrc.missouri.edu), an NIH-funded entity

469 whose mission is to generate transgenic swine models for biomedical research, engineered a
470 swine (the "Onco-pig"; mini-pig background) which carries an LSL-cassette containing
471 dominant negative *TP53* with a R167H mutation ($p53^{R167H}$) and activated $KRAS^{G12D}$ [*30, 44, 45*];
472 i.e., the porcine analog of the KRAS/p53 mouse [*42, 46*]. Site-specific expression of Cre
473 recombinase in the Onco-pig resulted in localized p53 inhibition and KRAS activation;
474 subcutaneous injection of AdCre produced mesenchymal tumors at the injection sites [*30*]. In
475 2017, initial work was published on a Onco-pig-based model of hepatocellular carcinoma [*90*].
476 All three of our cell lines demonstrated *in vitro* transformed behavior and the ability to
477 form tumors *in vivo*. Although we utilized a relatively high number of cells to obtain tumor
478 formation, we feel that this is due to the relative young age of our cell lines, which did not
479 undergo as many passages as other cell lines currently used to study pancreatic cancer. Thus, the
480 transformed cell lines in this report likely did not undergo an inadvertent selection for the fastest
481 growing cells, as may occur in older, extensively-passaged cell lines. Moreover, the lack of
482 desmoplasia in our murine xenograft model was not surprising, since most immunodeficient
483 murine models of pancreatic cancer do not recapitulate the extent of desmoplasia or metastasis
484 seen with human disease. We anticipate that future experiments involving the implantation of
485 transformed pancreatic ductal epithelial cells into wild type swine (and thus into a "normal"
486 microenvironment with "normal" immunoediting) will produce tumors with desmoplasia and
487 metastasis.
488
489

490 # References

491

492 1. American Cancer Society. Cancer Facts & Figures 2016. Atlanta: American Cancer
493 Society; 2016. Available from:
494 http://www.cancer.org/research/cancerfactsstatistics/cancerfactsfigures2016/index.
495 2. SEER (Surveillance, Epidemiology, and End Results Program) Stat Fact Sheets: Pancreas
496 Cancer: National Cancer Institute; [Accessed December 12, 2016]. Available from:
497 URL: http://seer.cancer.gov/statfacts/html/pancreas.html.
498 3. National Comprehensive Cancer Network. Pancreatic Adenocarcinoma, Version 2.2016.
499 2016. In: NCCN Clinical Practice Guidelines In Oncology (NCCN Guidelines®)
500 [Internet]. NCCN. Available from: www.nccn.org.
501 4. Costello E, Greenhalf W, Neoptolemos JP. New biomarkers and targets in pancreatic
502 cancer and their application to treatment. *Nat Rev Gastroenterol Hepatol*. 2012;9(8):435-
503 44. doi: 10.1038/nrgastro.2012.119. PubMed ID: 22733351; PubMed Central ID:
504 5. Seok J, Warren HS, Cuenca AG, Mindrinos MN, Baker HV, Xu W, et al. Genomic
505 responses in mouse models poorly mimic human inflammatory diseases. *PNAS*.
506 2013;110(9):3507-12. doi: 10.1073/pnas.1222878110. PubMed ID: 23401516; PubMed
507 Central ID:
508 6. Begley CG, Ellis LM. Drug development: Raise standards for preclinical cancer research.
509 *Nature*. 2012;483(7391):531-3. doi: 10.1038/483531a. PubMed ID: 22460880; PubMed
510 Central ID:

511 7. Cook N, Jodrell DI, Tuveson DA. Predictive in vivo animal models and translation to
512 clinical trials. *Drug Discov Today*. 2012;17(5-6):253-60. doi:
513 10.1016/j.drudis.2012.02.003. PubMed ID: 22493784; PubMed Central ID:
514 8. Le Magnen C, Dutta A, Abate-Shen C. Optimizing mouse models for precision cancer
515 prevention. *Nat Rev Cancer*. 2016;16(3):187-96. doi: 10.1038/nrc.2016.1. PubMed ID:
516 26893066; PubMed Central ID:
517 9. Reichert JM, Wenger JB. Development trends for new cancer therapeutics and vaccines.
518 *Drug Discov Today*. 2008;13(1-2):30-7. doi: 10.1016/j.drudis.2007.09.003. PubMed ID:
519 18190861; PubMed Central ID:
520 10. Sharpless NE, Depinho RA. The mighty mouse: genetically engineered mouse models in
521 cancer drug development. *Nat Rev Drug Discov*. 2006;5(9):741-54. doi:
522 10.1038/nrd2110. PubMed ID: 16915232; PubMed Central ID:
523 11. Ebos JM, Kerbel RS. Antiangiogenic therapy: impact on invasion, disease progression,
524 and metastasis. *Nat Rev Clin Oncol*. 2011;8(4):210-21. doi: 10.1038/nrclinonc.2011.21.
525 PubMed ID: 21364524; PubMed Central ID:
526 12. Francia G, Cruz-Munoz W, Man S, Xu P, Kerbel RS. Mouse models of advanced
527 spontaneous metastasis for experimental therapeutics. *Nat Rev Canc*. 2011;11(2):135-41.
528 doi: doi:10.1038/nrc3001. PubMed ID: 21258397; PubMed Central ID:
529 13. O'Collins VE, Macleod MR, Donnan GA, Horky LL, van der Worp BH, Howells DW.
530 1,026 experimental treatments in acute stroke. *Ann Neurol*. 2006;59(3):467-77. doi:
531 10.1002/ana.20741. PubMed ID: 16453316; PubMed Central ID:
532 14. Scott S, Kranz JE, Cole J, Lincecum JM, Thompson K, Kelly N, et al. Design, power,
533 and interpretation of studies in the standard murine model of ALS. *Amyotroph Lat Scler*.

534 2008;9(1):4-15. doi: 10.1080/17482960701856300. PubMed ID: 18273714; PubMed
535 Central ID:
536 15. Talmadge JE, Singh RK, Fidler IJ, Raz A. Murine models to evaluate novel and
537 conventional therapeutic strategies for cancer. *Am J Pathol*. 2007;170(3):793-804. doi:
538 10.2353/ajpath.2007.060929. PubMed ID: 17322365; PubMed Central ID: 1864878.
539 16. Rogers CS, Stoltz DA, Meyerholz DK, Ostedgaard LS, Rokhlina T, Taft PJ, et al.
540 Disruption of the CFTR gene produces a model of cystic fibrosis in newborn pigs.
541 *Science*. 2008;321(5897):1837-41. doi: 10.1126/science.1163600. PubMed ID:
542 18818360; PubMed Central ID: PMC2570747.
543 17. Flisikowska T, Merkl C, Landmann M, Eser S, Rezaei N, Cui X, et al. A porcine model
544 of familial adenomatous polyposis. *Gastroenterology*. 2012;143:1173-5. doi:
545 10.1053/j.gastro.2012.07.110. PubMed ID: 22864254; PubMed Central ID:
546 18. Pezzulo AA, Tang XX, Hoegger MJ, Abou Alaiwa MH, Ramachandran S, Moninger TO,
547 et al. Reduced airway surface pH impairs bacterial killing in the porcine cystic fibrosis
548 lung. *Nature*. 2012;487(7405):109-13. doi: 10.1038/nature11130. PubMed ID: 22763554;
549 PubMed Central ID: PMC3390761.
550 19. Maddalo D, Manchado E, Concepcion CP, Bonetti C, Vidigal JA, Han YC, et al. In vivo
551 engineering of oncogenic chromosomal rearrangements with the CRISPR/Cas9 system.
552 *Nature*. 2014;516(7531):423-7. doi: 10.1038/nature13902. PubMed ID: 25337876;
553 PubMed Central ID: PMC4270925.
554 20. Sanchez-Rivera FJ, Papagiannakopoulos T, Romero R, Tammela T, Bauer MR, Bhutkar
555 A, et al. Rapid modelling of cooperating genetic events in cancer through somatic

556 genome editing. *Nature*. 2014;516(7531):428-31. doi: 10.1038/nature13906. PubMed ID:
557 25337879; PubMed Central ID: PMC4292871.
558 21. Day CP, Merlino G, Van Dyke T. Preclinical mouse cancer models: a maze of
559 opportunities and challenges. *Cell*. 2015;163(1):39-53. doi: 10.1016/j.cell.2015.08.068.
560 PubMed ID: 26406370; PubMed Central ID: PMC4583714.
561 22. Singh M, Murriel CL, Johnson L. Genetically engineered mouse models: closing the gap
562 between preclinical data and trial outcomes. *Cancer Res*. 2012;72(11):2695-700. doi:
563 10.1158/0008-5472.CAN-11-2786. PubMed ID: 22593194; PubMed Central ID:
564 23. Zitvogel L, Pitt JM, Daillere R, Smyth MJ, Kroemer G. Mouse models in
565 oncoimmunology. *Nat Rev Cancer*. 2016;16(12):759-73. doi: 10.1038/nrc.2016.91.
566 PubMed ID: 27687979; PubMed Central ID:
567 24. Kilkenny C, Browne WJ, Cuthill IC, Emerson M, Altman DG. Improving bioscience
568 research reporting: the ARRIVE guidelines for reporting animal research. *PLoS Biol*.
569 2010;8(6):e1000412. doi: 10.1371/journal.pbio.1000412. PubMed ID: 20613859;
570 PubMed Central ID: PMC2893951.
571 25. National Institutes of Health. Principles and Guidelines for Reporting Preclinical
572 Research [February 5, 2016]. Available from: https://www.nih.gov/research-
573 training/rigor-reproducibility/principles-guidelines-reporting-preclinical-research.
574 26. National Institutes of Health. Enhancing Reproducibility through Rigor and
575 Transparency. NOT-OD-15-103. June 9, 2015. Available from:
576 http://grants.nih.gov/grants/guide/notice-files/NOT-OD-15-103.html.

577 27. Committee for the Update of the Guide for the Care and Use of Laboratory Animals.
578 *Guide for the Care and Use of Laboratory Animals*. Washington, DC: The National
579 Academies Press; 2011.
580 28. American Veterinary Medical Association Panel on Euthanasia. *AVMA Guidelines for the*
581 *Euthanasia of Animals: 2013 Edition*. Schaumberg, IL: American Veterinary Medical
582 Association; 2013.
583 29. Adam SJ, Rund LA, Kuzmuk KN, Zachary JF, Schook LB, Counter CM. Genetic
584 induction of tumorigenesis in swine. *Oncogene*. 2007;26(7):1038-45. doi:
585 10.1038/sj.onc.1209892. PubMed ID: 16964292; PubMed Central ID:
586 30. Schook LB, Collares TV, Hu W, Liang Y, Rodrigues FM, Rund LA, et al. A Genetic
587 Porcine Model of Cancer. *PLOS ONE*. 2015;10(7):e0128864. doi:
588 10.1371/journal.pone.0128864. PubMed ID: 26132737; PubMed Central ID:
589 PMC4488487.
590 31. Schmittgen TD, Livak KJ. Analyzing real-time PCR data by the comparative C(T)
591 method. *Nat Protoc*. 2008;3(6):1101-8. Epub 2008/06/13. PubMed ID: 18546601;
592 PubMed Central ID:
593 32. Grinnell F, Zhu M, Carlson MA, Abrams JM. Release of mechanical tension triggers
594 apoptosis of human fibroblasts in a model of regressing granulation tissue. *Exp Cell Res*.
595 1999;248(2):608-19. Epub 1999/05/01. doi: 10.1006/excr.1999.4440. PubMed ID:
596 10222153; PubMed Central ID:
597 33. Macpherson I, Montagnier L. Agar Suspension Culture for the Selective Assay of Cells
598 Transformed by Polyoma Virus. *Virology*. 1964;23:291-4. Epub 1964/06/01. PubMed ID:
599 14187925; PubMed Central ID:

600 34. Liang CC, Park AY, Guan JL. In vitro scratch assay: a convenient and inexpensive
601 method for analysis of cell migration in vitro. *Nat Protoc*. 2007;2(2):329-33. Epub
602 2007/04/05. doi: 10.1038/nprot.2007.30. PubMed ID: 17406593; PubMed Central ID:
603 35. Tsutsumida H, Swanson BJ, Singh PK, Caffrey TC, Kitajima S, Goto M, et al. RNA
604 interference suppression of MUC1 reduces the growth rate and metastatic phenotype of
605 human pancreatic cancer cells. *Clin Cancer Res*. 2006;12(10):2976-87. Epub 2006/05/19.
606 doi: 10.1158/1078-0432.CCR-05-1197. PubMed ID: 16707592; PubMed Central ID:
607 36. Gioviale MC, Damiano G, Montalto G, Buscemi G, Romano M, Lo Monte AI. Isolation
608 and culture of beta-like cells from porcine Wirsung duct. *Transplant Proc*.
609 2009;41(4):1363-6. doi: 10.1016/j.transproceed.2009.02.062. PubMed ID: 19460560;
610 PubMed Central ID:
611 37. Govindan R, Ding L, Griffith M, Subramanian J, Dees ND, Kanchi KL, et al. Genomic
612 landscape of non-small cell lung cancer in smokers and never-smokers. *Cell*.
613 2012;150(6):1121-34. doi: 10.1016/j.cell.2012.08.024. PubMed ID: 22980976; PubMed
614 Central ID: PMC3656590.
615 38. Kandoth C, McLellan MD, Vandin F, Ye K, Niu B, Lu C, et al. Mutational landscape and
616 significance across 12 major cancer types. *Nature*. 2013;502(7471):333-9. Epub
617 2013/10/18. doi: 10.1038/nature12634. PubMed ID: 24132290; PubMed Central ID:
618 39. Stephens PJ, Tarpey PS, Davies H, Van Loo P, Greenman C, Wedge DC, et al. The
619 landscape of cancer genes and mutational processes in breast cancer. *Nature*.
620 2012;486(7403):400-4. PubMed ID: 22722201; PubMed Central ID:

621 40. Vogelstein B, Papadopoulos N, Velculescu VE, Zhou S, Diaz LA, Jr., Kinzler KW.
622 Cancer genome landscapes. *Science*. 2013;339(6127):1546-58. doi:
623 10.1126/science.1235122. PubMed ID: 23539594; PubMed Central ID: 3749880.
624 41. Waddell N, Pajic M, Patch AM, Chang DK, Kassahn KS, Bailey P, et al. Whole genomes
625 redefine the mutational landscape of pancreatic cancer. *Nature*. 2015;518:495-501. doi:
626 10.1038/nature14169. PubMed ID: PMC4523082; PubMed Central ID:
627 42. Hingorani SR, Wang L, Multani AS, Combs C, Deramaudt TB, Hruban RH, et al.
628 Trp53R172H and KrasG12D cooperate to promote chromosomal instability and widely
629 metastatic pancreatic ductal adenocarcinoma in mice. *Cancer Cell*. 2005;7(5):469-83.
630 Epub 2005/05/17. doi: 10.1016/j.ccr.2005.04.023. PubMed ID: 15894267; PubMed
631 Central ID:
632 43. Groenen MA, Archibald AL, Uenishi H, Tuggle CK, Takeuchi Y, Rothschild MF, et al.
633 Analyses of pig genomes provide insight into porcine demography and evolution. *Nature*.
634 2012;491(7424):393-8. doi: 10.1038/nature11622. PubMed ID: 23151582; PubMed
635 Central ID:
636 44. Rodrigues F, Hu W, Rund L, Liang Y, Counter C, Schook L. Development of the "Onco-
637 Pig": An Inducible Transgenic Porcine Model for Human Cancer [poster]. 2013
638 Brazilian Genetics Conference; URL:
639 http://www.dbs.illinois.edu/comparativegenomics/userfiles/file/ocnopigPoster_Brazilian
640 %20Genetics%20Conference2013.pdf.
641 45. . Conference Proceedings: Swine in Biomedical Research; July 6-8, 2014; Raleigh, NC.

642 46. DuPage M, Dooley AL, Jacks T. Conditional mouse lung cancer models using adenoviral
643 or lentiviral delivery of Cre recombinase. *Nat Protoc*. 2009;4(7):1064-72. doi:
644 10.1038/nprot.2009.95. PubMed ID: 19561589; PubMed Central ID:
645 47. Bailey JM, Swanson BJ, Hamada T, Eggers JP, Singh PK, Caffery T, et al. Sonic
646 hedgehog promotes desmoplasia in pancreatic cancer. *Clin Cancer Res*.
647 2008;14(19):5995-6004. Epub 2008/10/03. doi: 10.1158/1078-0432.CCR-08-0291.
648 PubMed ID: 18829478; PubMed Central ID: PMC2782957.
649 48. Handra-Luca A, Hong SM, Walter K, Wolfgang C, Hruban R, Goggins M. Tumour
650 epithelial vimentin expression and outcome of pancreatic ductal adenocarcinomas. *Br J*
651 *Cancer*. 2011;104(8):1296-302. Epub 2011/03/31. doi: 10.1038/bjc.2011.93. PubMed ID:
652 21448168; PubMed Central ID: PMC3078601.
653 49. Kheirabadi BS, Mace JE, Terrazas IB, Fedyk CG, Estep JS, Dubick MA, et al. Safety
654 evaluation of new hemostatic agents, smectite granules, and kaolin-coated gauze in a
655 vascular injury wound model in swine. *J Trauma*. 2010;68(2):269-78. doi:
656 10.1097/TA.0b013e3181c97ef1. PubMed ID: 20154537; PubMed Central ID:
657 50. Cooper DK, Ekser B, Ramsoondar J, Phelps C, Ayares D. The role of genetically
658 engineered pigs in xenotransplantation research. *J Pathol*. 2016;238(2):288-99. doi:
659 10.1002/path.4635. PubMed ID: 26365762; PubMed Central ID: PMC4689670.
660 51. Sullivan TP, Eaglstein WH, Davis SC, Mertz P. The pig as a model for human wound
661 healing. *Wound Repair Regen*. 2001;9(2):66-76. doi: 10.1046/j.1524-475x.2001.00066.x.
662 PubMed ID: 11350644; PubMed Central ID:
663 52. Swindle MM, Makin A, Herron AJ, Clubb FJ, Jr., Frazier KS. Swine as models in
664 biomedical research and toxicology testing. *Vet Pathol*. 2012;49(2):344-56. Epub

665 2011/03/29. doi: 10.1177/0300985811402846. PubMed ID: 21441112; PubMed Central
666 ID:
667 53. Xiangdong L, Yuanwu L, Hua Z, Liming R, Qiuyan L, Ning L. Animal models for the
668 atherosclerosis research: a review. *Protein Cell*. 2011;2(3):189-201. doi: 10.1007/s13238-
669 011-1016-3. PubMed ID: 21468891; PubMed Central ID: PMC4875304.
670 54. Gouadon E, Moore-Morris T, Smit NW, Chatenoud L, Coronel R, Harding SE, et al.
671 Concise Review: Pluripotent Stem Cell-Derived Cardiac Cells, A Promising Cell Source
672 for Therapy of Heart Failure: Where Do We Stand? *Stem Cells*. 2016;34(1):34-43. doi:
673 10.1002/stem.2205. PubMed ID: 26352327; PubMed Central ID:
674 55. Kuzmuk KN, Schook LB. Pigs as a Model for Biomedical Sciences. In: Rothschild MF,
675 Ruvinsky A, editors. *The Genetics of the Pig*. Oxfordshire, UK: CABI; 2011. p. 426-44.
676 56. Emes RD, Goodstadt L, Winter EE, Ponting CP. Comparison of the genomes of human
677 and mouse lays the foundation of genome zoology. *Hum Mol Genet*. 2003;12(7):701-9.
678 doi: 10.1093/hmg/ddg078. PubMed ID: 12651866; PubMed Central ID:
679 57. Walters E, Wolf E, Whyte J, Mao J, Renner S, Nagashima H, et al. Completion of the
680 swine genome will simplify the production of swine as a large animal biomedical model.
681 *BMC Med Genom*. 2012;5(1):55. doi: 10.1186/1755-8794-5-55. PubMed ID: 23151353;
682 PubMed Central ID:
683 58. Dawson HD, McAnulty P, Dayan A, Ganderup N, Hastings K. A comparative assessment
684 of the pig, mouse and human genomes. In: McAnulty P, Dayan A, Ganderup N, Hastings
685 K, editors. *The Minipig in Biomedical Research*. Boca Raton, FL: CRC Press; 2012. p.
686 323-42.

687 59. Dawson HD, Smith AD, Chen C, Urban JF, Jr. An in-depth comparison of the porcine,
688 murine and human inflammasomes; lessons from the porcine genome and transcriptome.
689 *Vet Microbiol*. 2017;202:2-15. Epub 2016/06/21. doi: 10.1016/j.vetmic.2016.05.013.
690 PubMed ID: 27321134; PubMed Central ID:
691 60. Schachtschneider KM, Madsen O, Park C, Rund LA, Groenen MA, Schook LB. Adult
692 porcine genome-wide DNA methylation patterns support pigs as a biomedical model.
693 *BMC Genomics*. 2015;16:743. Epub 2015/10/07. doi: 10.1186/s12864-015-1938-x.
694 PubMed ID: 26438392; PubMed Central ID: PMC4594891.
695 61. Vodicka P, Smetana K, Jr., Dvorankova B, Emerick T, Xu YZ, Ourednik J, et al. The
696 miniature pig as an animal model in biomedical research. *Ann N Y Acad Sci*.
697 2005;1049:161-71. Epub 2005/06/21. doi: 10.1196/annals.1334.015. PubMed ID:
698 15965115; PubMed Central ID:
699 62. Swindle MM, Smith AC. *Swine in the Laboratory: Surgery, Anesthesia, Imaging, and*
700 *Experimental Techniques*. 3rd ed. Boca Raton, FL: CRC Press; 2016.
701 63. Spurlock ME, Gabler NK. The development of porcine models of obesity and the
702 metabolic syndrome. *J Nutr*. 2008;138(2):397-402. Epub 2008/01/22. PubMed ID:
703 18203910; PubMed Central ID:
704 64. Röthkotter HJ. Anatomical particularities of the porcine immune system--a physician's
705 view. *Dev Comp Immunol*. 2009;33(3):267-72. doi: 10.1016/j.dci.2008.06.016. PubMed
706 ID: 18775744; PubMed Central ID:
707 65. Bailey M. The mucosal immune system: recent developments and future directions in the
708 pig. *Dev Comp Immunol*. 2009;33(3):375-83. doi: 10.1016/j.dci.2008.07.003. PubMed
709 ID: 18760299; PubMed Central ID:

710 66. Fairbairn L, Kapetanovic R, Sester DP, Hume DA. The mononuclear phagocyte system
711 of the pig as a model for understanding human innate immunity and disease. *J Leukoc*
712 *Biol*. 2011;89(6):855-71. doi: 10.1189/jlb.1110607. PubMed ID: 21233410; PubMed
713 Central ID:
714 67. Meurens F, Summerfield A, Nauwynck H, Saif L, Gerdts V. The pig: a model for human
715 infectious diseases. *Trends Microbiol*. 2012;20(1):50-7. doi: 10.1016/j.tim.2011.11.002.
716 PubMed ID: 22153753; PubMed Central ID:
717 68. Petersen B, Carnwath JW, Niemann H. The perspectives for porcine-to-human
718 xenografts. *Comp Immunol Microbiol Infect Dis*. 2009;32(2):91-105. doi:
719 10.1016/j.cimid.2007.11.014. PubMed ID: 18280567; PubMed Central ID:
720 69. Ferrer J, Scott WE, 3rd, Weegman BP, Suszynski TM, Sutherland DE, Hering BJ, et al.
721 Pig pancreas anatomy: implications for pancreas procurement, preservation, and islet
722 isolation. *Transplantation*. 2008;86(11):1503-10. doi: 10.1097/TP.0b013e31818bfda1.
723 PubMed ID: 19077881; PubMed Central ID: 2704055.
724 70. Gun G, Kues WA. Current progress of genetically engineered pig models for biomedical
725 research. *Biores Open Access*. 2014;3(6):255-64. doi: 10.1089/biores.2014.0039.
726 PubMed ID: 25469311; PubMed Central ID: 4245835.
727 71. Fan N, Lai L. Genetically modified pig models for human diseases. *J Genet Genomics*.
728 2013;40(2):67-73. doi: 10.1016/j.jgg.2012.07.014. PubMed ID: 23439405; PubMed
729 Central ID:
730 72. Prather RS, Lorson M, Ross JW, Whyte JJ, Walters E. Genetically engineered pig models
731 for human diseases. *Annu Rev Anim Biosci*. 2013;1:203-19. doi: 10.1146/annurev-animal-
732 031412-103715. PubMed ID: 25387017; PubMed Central ID:

733 73. Luo Y, Li J, Liu Y, Lin L, Du Y, Li S, et al. High efficiency of BRCA1 knockout using
734 rAAV-mediated gene targeting: developing a pig model for breast cancer. *Transgenic*
735 *Res*. 2011;20(5):975-88. doi: 10.1007/s11248-010-9472-8. PubMed ID: 21181439;
736 PubMed Central ID:
737 74. Luo Y, Bolund L, Sorensen CB. Pig gene knockout by rAAV-mediated homologous
738 recombination: comparison of BRCA1 gene knockout efficiency in Yucatan and
739 Gottingen fibroblasts with slightly different target sequences. *Transgenic Res*.
740 2012;21(3):671-6. doi: 10.1007/s11248-011-9563-1. PubMed ID: 22020980; PubMed
741 Central ID:
742 75. Leuchs S, Saalfrank A, Merkl C, Flisikowska T, Edlinger M, Durkovic M, et al.
743 Inactivation and inducible oncogenic mutation of p53 in gene targeted pigs. *PLoS ONE*.
744 2012;7(10):e43323. doi: 10.1371/journal.pone.0043323. PubMed ID: 23071491; PubMed
745 Central ID:
746 76. Sieren JC, Meyerholz DK, Wang XJ, Davis BT, Newell JD, Jr., Hammond E, et al.
747 Development and translational imaging of a TP53 porcine tumorigenesis model. *J Clin*
748 *Invest*. 2014;124(9):4052-66. doi: 10.1172/JCI75447. PubMed ID: 25105366; PubMed
749 Central ID: 4151205.
750 77. Yang L, Guell M, Niu D, George H, Lesha E, Grishin D, et al. Genome-wide inactivation
751 of porcine endogenous retroviruses (PERVs). *Science*. 2015;350(6264):1101-4. Epub
752 2015/10/13. doi: 10.1126/science.aad1191. PubMed ID: 26456528; PubMed Central ID:
753 78. Beraldi R, Meyerholz D, Savinov A, Kovács A, Weimer J, Dykstra J, et al. Genetic
754 Ataxia Telangiectasia porcine model phenocopies the multisystemic features of the

755 human disease. *Biochim Biophys Acta*. 2017:ePub ahead of print, 2017 Jul 23. doi:
756 10.1016/j.bbadis.2017.07.020. PubMed ID: 28746835; PubMed Central ID:
757 79. Smit VT, Boot AJ, Smits AM, Fleuren GJ, Cornelisse CJ, Bos JL. KRAS codon 12
758 mutations occur very frequently in pancreatic adenocarcinomas. *Nucleic Acids Res*.
759 1988;16(16):7773-82. PubMed ID: 3047672; PubMed Central ID: PMC338489.
760 80. Jones S, Zhang X, Parsons DW, Lin JC, Leary RJ, Angenendt P, et al. Core signaling
761 pathways in human pancreatic cancers revealed by global genomic analyses. *Science*.
762 2008;321(5897):1801-6. doi: 10.1126/science.1164368. PubMed ID: 18772397; PubMed
763 Central ID: PMC2848990.
764 81. Muller PA, Vousden KH. p53 mutations in cancer. *Nat Cell Biol*. 2013;15(1):2-8. doi:
765 10.1038/ncb2641. PubMed ID: 23263379; PubMed Central ID:
766 82. Olivier M, Hollstein M, Hainaut P. TP53 mutations in human cancers: origins,
767 consequences, and clinical use. *Cold Spring Harbor Perspectives in Biology*. 2010;2(1).
768 doi: 10.1101/cshperspect.a001008. PubMed ID: 20182602; PubMed Central ID:
769 83. Blackford A, Serrano OK, Wolfgang CL, Parmigiani G, Jones S, Zhang X, et al. SMAD4
770 gene mutations are associated with poor prognosis in pancreatic cancer. *Clin Cancer Res*.
771 2009;15(14):4674-9. doi: 10.1158/1078-0432.CCR-09-0227. PubMed ID: 19584151;
772 PubMed Central ID: PMC2819274.
773 84. Caldas C, Hahn SA, da Costa LT, Redston MS, Schutte M, Seymour AB, et al. Frequent
774 somatic mutations and homozygous deletions of the p16 (MTS1) gene in pancreatic
775 adenocarcinoma. *Nat Genet*. 1994;8(1):27-32. doi: 10.1038/ng0994-27. PubMed ID:
776 7726912; PubMed Central ID:

777 85. Bardeesy N, Cheng KH, Berger JH, Chu GC, Pahler J, Olson P, et al. Smad4 is
778 dispensable for normal pancreas development yet critical in progression and tumor
779 biology of pancreas cancer. *Genes Dev*. 2006;20(22):3130-46. doi: 10.1101/gad.1478706.
780 PubMed ID: 17114584; PubMed Central ID: PMC1635148.
781 86. Bardeesy N, Aguirre AJ, Chu GC, Cheng KH, Lopez LV, Hezel AF, et al. Both
782 p16(Ink4a) and the p19(Arf)-p53 pathway constrain progression of pancreatic
783 adenocarcinoma in the mouse. *Proc Natl Acad Sci U S A*. 2006;103(15):5947-52. doi:
784 10.1073/pnas.0601273103. PubMed ID: 16585505; PubMed Central ID: PMC1458678.
785 87. Flisikowska T, Kind A, Schnieke A. The new pig on the block: modelling cancer in pigs.
786 *Transgenic Res*. 2013;22(4):673-80. doi: 10.1007/s11248-013-9720-9. PubMed ID:
787 23748932; PubMed Central ID:
788 88. Ittmann M, Huang J, Radaelli E, Martin P, Signoretti S, Sullivan R, et al. Animal Models
789 of Human Prostate Cancer: The Consensus Report of the New York Meeting of the
790 Mouse Models of Human Cancers Consortium Prostate Pathology Committee. *Canc Res*.
791 2013;73(9):2718-36. doi: 10.1158/0008-5472.CAN-12-4213. PubMed ID: 23610450;
792 PubMed Central ID:
793 89. Luo Y, Kofod-Olsen E, Christensen R, Sorensen CB, Bolund L. Targeted genome editing
794 by recombinant adeno-associated virus (rAAV) vectors for generating genetically
795 modified pigs. *J Gen Genom*. 2012;39(6):269-74. doi: 10.1016/j.jgg.2012.05.004.
796 PubMed ID: 22749014; PubMed Central ID:
797 90. Schachtschneider K, Schwind R, Darfour-Oduro K, De A, Rund L, Singh K, et al. A
798 validated, transitional and translational porcine model of hepatocellular carcinoma.

Oncotarget. 2017:Epub ahead of print, 2017 Jun 29. Epub 2017 Jun 29. doi: 10.18632/oncotarget.18872. PubMed ID: 28733541; PubMed Central ID:

804 # Acknowledgements

805

806 This study is the result of work supported in part with resources and the use of facilities
807 at the Omaha VA Medical Center (Nebraska-Western Iowa Health Care System). Portions of this
808 study were presented at the 108th Annual Meeting of the American Association for Cancer
809 Research (AACR) in Washington, D.C., April 1-5, 2017. The authors would like to acknowledge
810 the technical assistance of Gerri Siford, Chris Hansen, Kelly O'Connell, and Tom Caffrey. The
811 authors also would like to thank Dr. Lawrence B. Schook and Dr. Laurie A. Rund at the
812 University of Illinois for the gift of their plasmid that contained the *KRAS*^{G12D} mutation, along
813 with comments, insights and suggestions for its use in this project.

814

815

Author Contributions

Contributor Role	Description	Author
Conceptualization	Ideas; formulation or evolution of overarching research goals and aims.	MAC
Data Curation	Management activities to annotate (produce metadata), scrub data and maintain research data (including software code, where it is necessary for interpreting the data itself) for initial use and later reuse.	NR, JLC, JAG
Formal Analysis	Application of statistical, mathematical, computational, or other formal techniques to analyze or synthesize study data.	NR, MAC
Funding Acquisition	Acquisition of the financial support for the project leading to this publication.	MAC
Investigation	Conducting a research and investigation process, specifically performing the experiments, or data/evidence collection.	NR, JLC, JAG, MAC
Methodology	Development or design of methodology; creation of models.	NR, MAH, MAC
Project Administration	Management and coordination responsibility for the research activity planning and execution.	MAC
Resources	Provision of study materials, reagents, materials, patients, laboratory samples, animals, instrumentation, computing resources, or other analysis tools.	MAH, MAC
Software	Programming, software development; designing computer programs; implementation of the computer code and supporting algorithms; testing of existing code components.	na
Supervision	Oversight and leadership responsibility for the research activity planning and execution, including mentorship external to the core team.	MAH, MAC
Validation	Verification, whether as a part of the activity or separate, of the overall replication/reproducibility of results/experiments and other research outputs.	NR, JLC, JAG
Visualization	Preparation, creation and/or presentation of the published work, specifically visualization/data presentation.	NR, MAC
Draft Preparation	Creation and/or presentation of the published work, specifically writing the initial draft (including substantive translation).	NR, MAC
Review & Editing	Preparation, creation and/or presentation of the published work by those from the original research group, specifically critical review, commentary or revision – including pre- or post-publication stages.	NR, JLC, JAG, MAH, MAC

na = not applicable.

820 **Table 1. Tumorigenic cell lines and their expression products.**
821

Cell line	AcGFP1 protein	$KRAS^{G12D}$ protein	$p53^{R167H}$ protein	SMAD4 shRNA	$p16^{Ink4A}$ shRNA
PGKP	+	+	+		
PGKPS	+	+	+	+	
PGKPSC*	+	+	+	+	+

822
823 All cell lines based on primary porcine pancreatic ductal epithelial cells. *Abbreviation key: **P** =
824 pancreatic ductal epithelium; **G** = GFP; **K** = KRAS; **P** = p53; **S** = SMAD4; **C** =
825 $p16^{Ink4A}$/CDKN2A.
826

827 **Figure Legends**

828

829 **Fig. 1. Isolation and transduction of primary porcine pancreatic ductal epithelial cells.** (A)
830 Phase image of cells isolated from porcine pancreatic duct, showing epithelial-like morphology
831 (bar = 1,000 µm). (B) Immunofluorescent staining for cytokeratin 19 in the cultured primary
832 cells (bar = 200 µm). (C) Immunoblot for the p53 mutant in nine different cells lines transduced
833 with the GKP virus (PGKP cells). Pancreas = wild type pancreatic ductal epithelial cells.
834 Representative blot of three separate experiments. (D-E) qPCR of KRAS and p53 mutants in the
835 nine PKGP cell lines. Each bar represents mean of three separate experiments. *$p<0.05$, **
836 $p<0.03$, ***$p<0.01$ (unpaired t-test, compared to wild type).

837

838 **Fig. 2. Effect of SMAD4 and $p16^{Ink4A}$ knockdown on transformation in the PGKP cell line.**
839 (A) Soft agar assay and (B) migration assay in the nine GKP-transduced cell lines. Pancreas =
840 wild type pancreatic ductal epithelial cells. Each bar represents mean of three separate
841 experiments. (C) RT-PCR of SMAD4 and $p16^{Ink4A}$/CDKN2A mRNA in cell lines expressing
842 targeted or scramble shRNA. Representative blot of three separate experiments. (D) Soft agar
843 assay and (E) migration assay of selected cell lines (PGKP, PGKPS, and PGKPSC), showing the
844 *in vitro* effect of additional knockdown of SMAD4 ± $p16^{Ink4A}$ on the transformation of GKP-
845 transduced pancreatic ductal epithelial cells.

846

847 **Fig. 3. *In vitro* transformation assays comparing the PGKP, PGKPS, and PGKPSC cell**
848 **lines**. (A) Cell culture population doubling time (count-based assay). Pancreas = wild type
849 pancreatic ductal epithelial cells. (B) Proliferation rate (metabolic dye-based assay), represented

850 as fold change, normalized to wild type cells. (C) Invasion (Matrigel®-based assay). Each bar or
851 data point represents mean of three separate experiments.
852
853 **Fig. 4. *In vivo* tumorigenesis assays comparing the PGKP, PGKPS, and PGKPSC cell lines**.
854 (A) Sample of a resected tumor from subcutaneous injection in nude mice; note size and
855 vascularity. (B) Tumor growth curve from the subcutaneous injection in nude mice. Each data
856 point represents mean of 10 mice. (C) Metastasis after orthotopic implantation in nude mice
857
858 **Fig. 5. Tumor immunohistochemistry from subcutaneous nude mouse assay.** Representative
859 images of primary tumors derived from the PGKP, PGKPS, and PGKPSC cell lines stained with
860 an array of epithelial markers, including E-cadherin (Ecad; B, G, L), Epithelial Cell Adhesion
861 Molecule (EpCAM; C, H, M), Pan-Cytokeratin (PanCK; D, I, N), and Cytokeratin-19 (CK19; E,
862 J, O); and also stained with mesenchymal markers, including α-Smooth Muscle Actin (SMA; P,
863 S, V), Vimentin (Vim; Q, T, W), and Type I Collagen (Col I; R, U, X). Bar = 200 μm.
864

865 # Supporting Information

866

867 [upload pending]

868

869 **Fig. S1**. pIRES2-AcGFP1 Vector Information

870 **Fig. S2**. Onco-pig

871 **Fig. S3**. KRAS/p53 immunohistochemistry of subcutaneous murine tumors

872 **Protocol**: Isolation of Epithelial Cells from Porcine Pancreas

873 **Table S1**. Responses to the ARRIVE recommendations

874 **Table S2**. Responses to the NIH Preclinical Research Guidelines

875 **Table S3**. Primers and other short sequences

876 **Table S4**. Antibody information

877

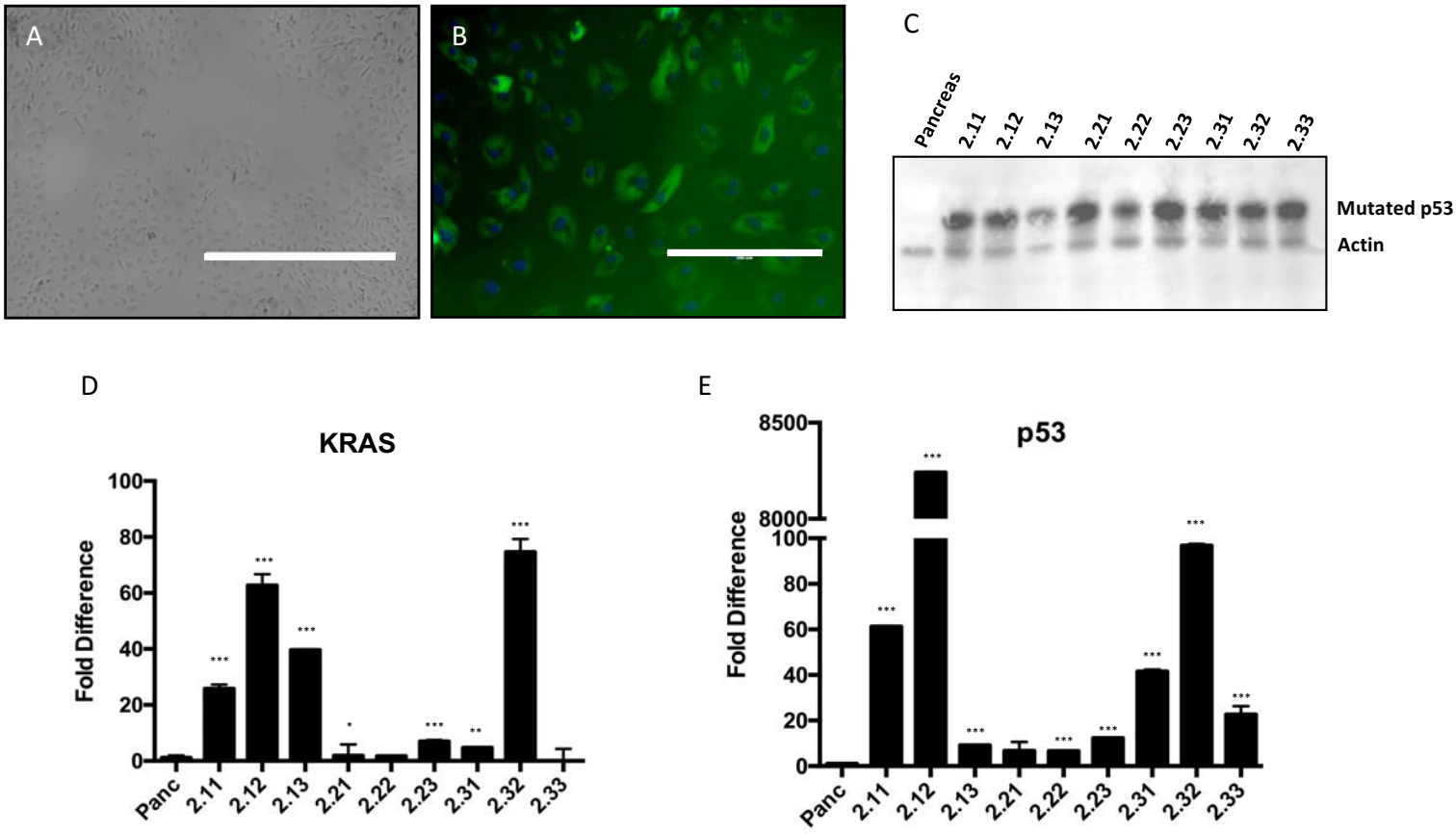
A
B
C
Pancreas
2.11
2.12
2.13
2.21
2.22
2.23
2.31
2.32
2.33
Mutated p53
Actin
D
KRAS
Fold Difference
100
80
60
40
20
0
Panc
2.11
2.12
2.13
2.21
2.22
2.23
2.31
2.32
2.33
E
p53
Fold Difference
8500
8000
100
80
60
40
20
0
Panc
2.11
2.12
2.13
2.21
2.22
2.23
2.31
2.32
2.33

Figure 1

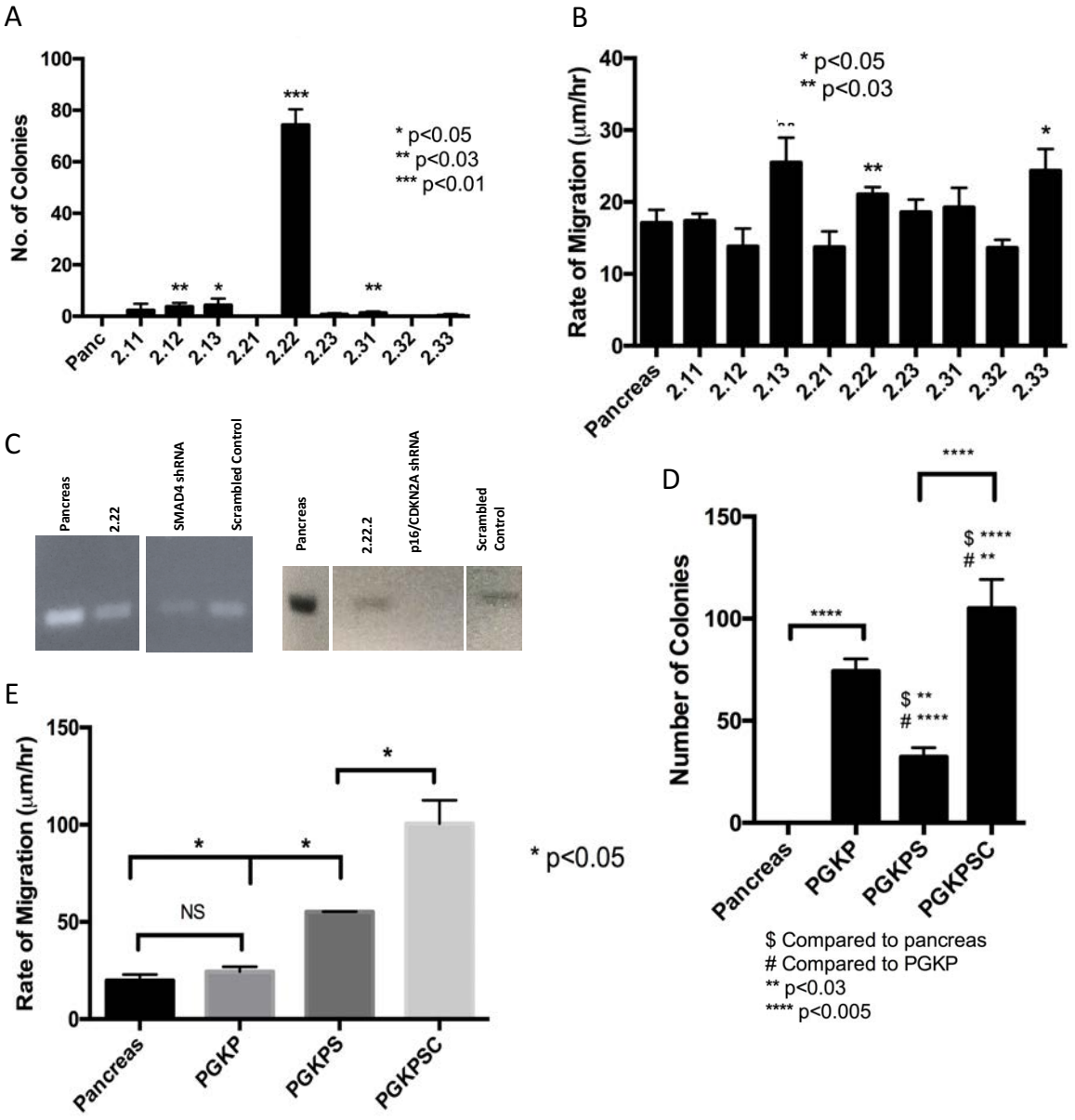
A
No. of Colonies
100
80
60
40
20
0
***
**
*
**
* p<0.05
** p<0.03
*** p<0.01
Panc
2.11
2.12
2.13
2.21
2.22
2.23
2.31
2.32
2.33
B
Rate of Migration (μm/hr)
40
30
20
10
0
* p<0.05
** p<0.03
**
*
Pancreas
2.11
2.12
2.13
2.21
2.22
2.23
2.31
2.32
2.33
C
Pancreas
2.22
SMAD4 shRNA
Scrambled Control
Pancreas
2.22.2
p16/CDKN2A shRNA
Scrambled Control
D
Number of Colonies
150
100
50
0
****
****
$ ****
# **
$ **
# ****
Pancreas
PGKP
PGKPS
PGKPSC
$ Compared to pancreas
# Compared to PGKP
** p<0.03
**** p<0.005
E
Rate of Migration (μm/hr)
150
100
50
0
*
*
*
NS
* p<0.05
Pancreas
PGKP
PGKPS
PGKPSC

Figure 2

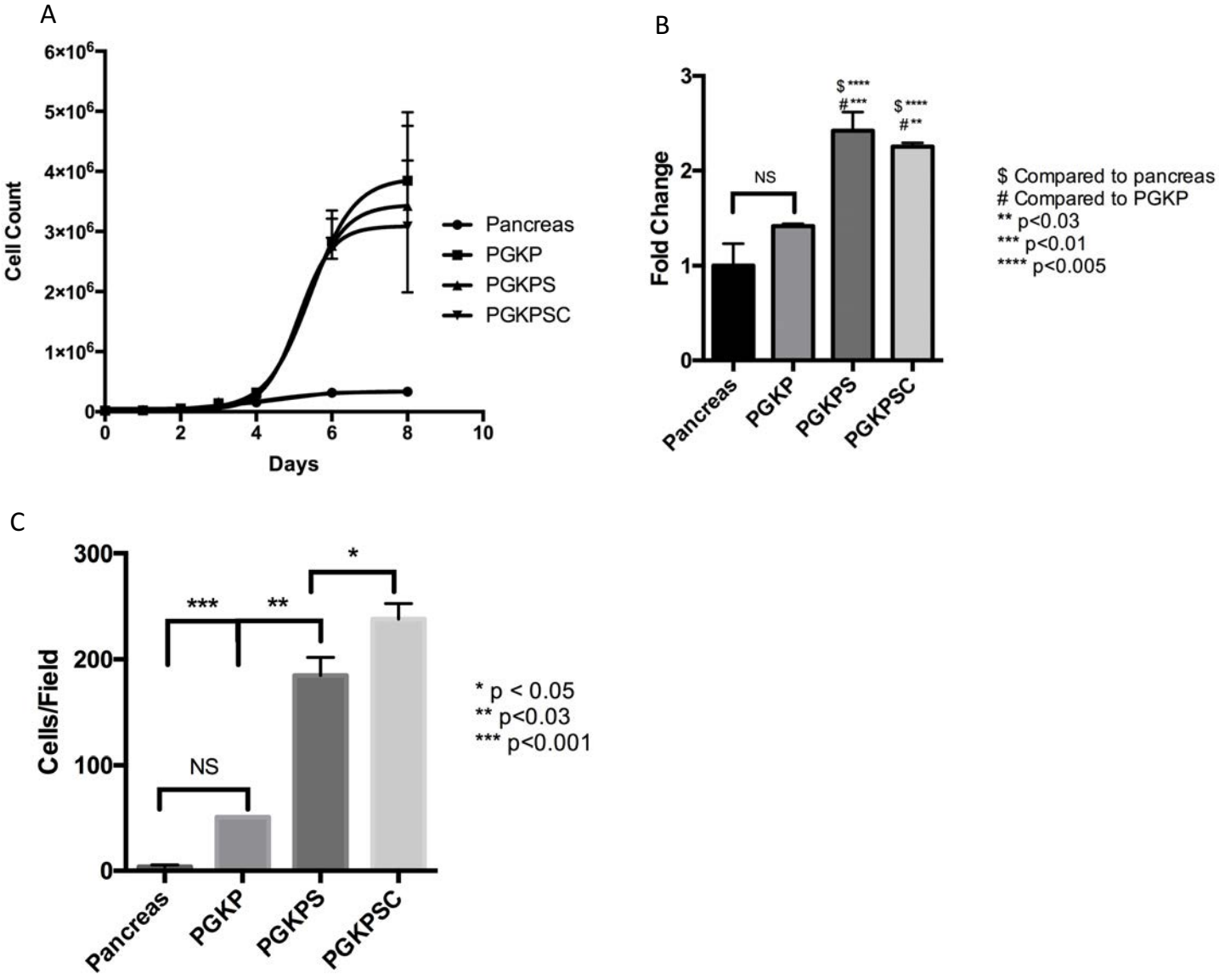
A
Cell Count
6×10^6
5×10^6
4×10^6
3×10^6
2×10^6
1×10^6
0
0
2
4
6
8
10
Days
Pancreas
PGKP
PGKPS
PGKPSC
B
Fold Change
3
2
1
0
NS
$ ****
# ***
$ ****
# **
Pancreas
PGKP
PGKPS
PGKPSC
$ Compared to pancreas
# Compared to PGKP
** p<0.03
*** p<0.01
**** p<0.005
C
Cells/Field
300
200
100
0
***
**
*
NS
Pancreas
PGKP
PGKPS
PGKPSC
* p < 0.05
** p<0.03
*** p<0.001

Figure 3

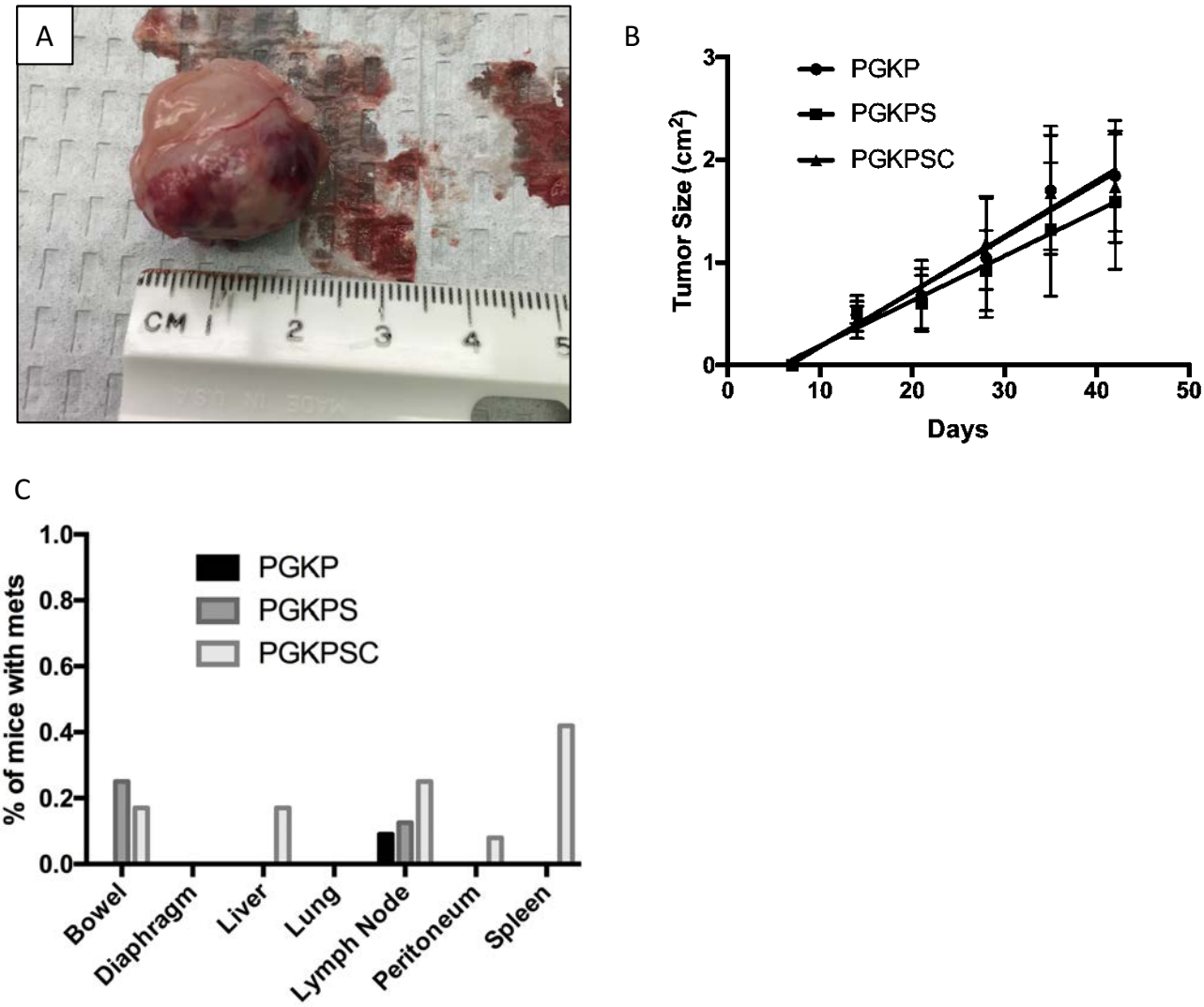
A
CM 1 2 3 4 5
B
PGKP
PGKPS
PGKPSC
Tumor Size (cm2)
Days
0
10
20
30
40
50
0
1
2
3
C
PGKP
PGKPS
PGKPSC
% of mice with mets
0.0
0.2
0.4
0.6
0.8
1.0
Bowel
Diaphragm
Liver
Lung
Lymph Node
Peritoneum
Spleen

Figure 4

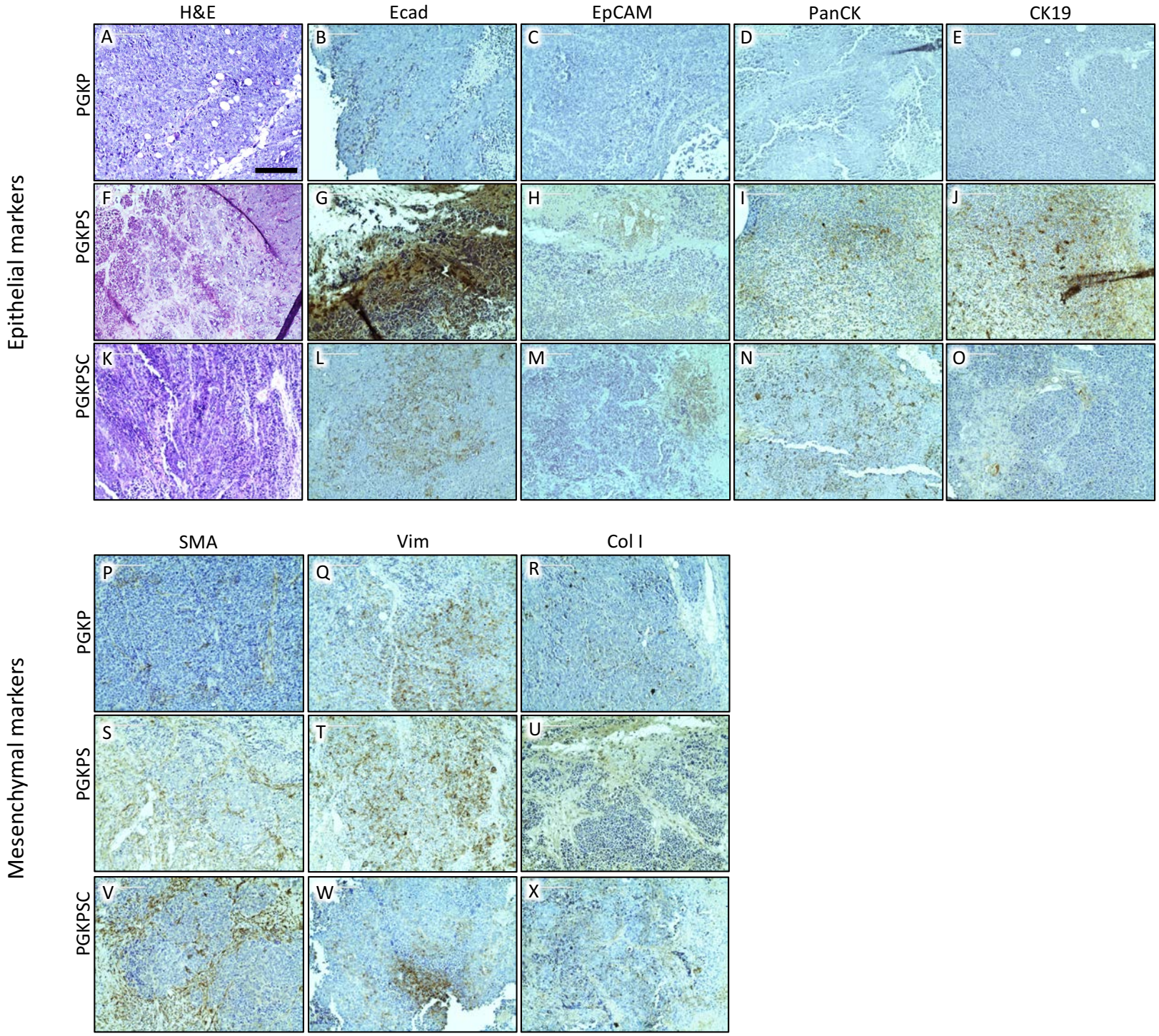
H&E
Ecad
EpCAM
PanCK
CK19
Epithelial markers
PGKP
PGKPS
PGKPSC
A
B
C
D
E
F
G
H
I
J
K
L
M
N
O
SMA
Vim
Col I
Mesenchymal markers
P
Q
R
S
T
U
V
W
X

Figure 5

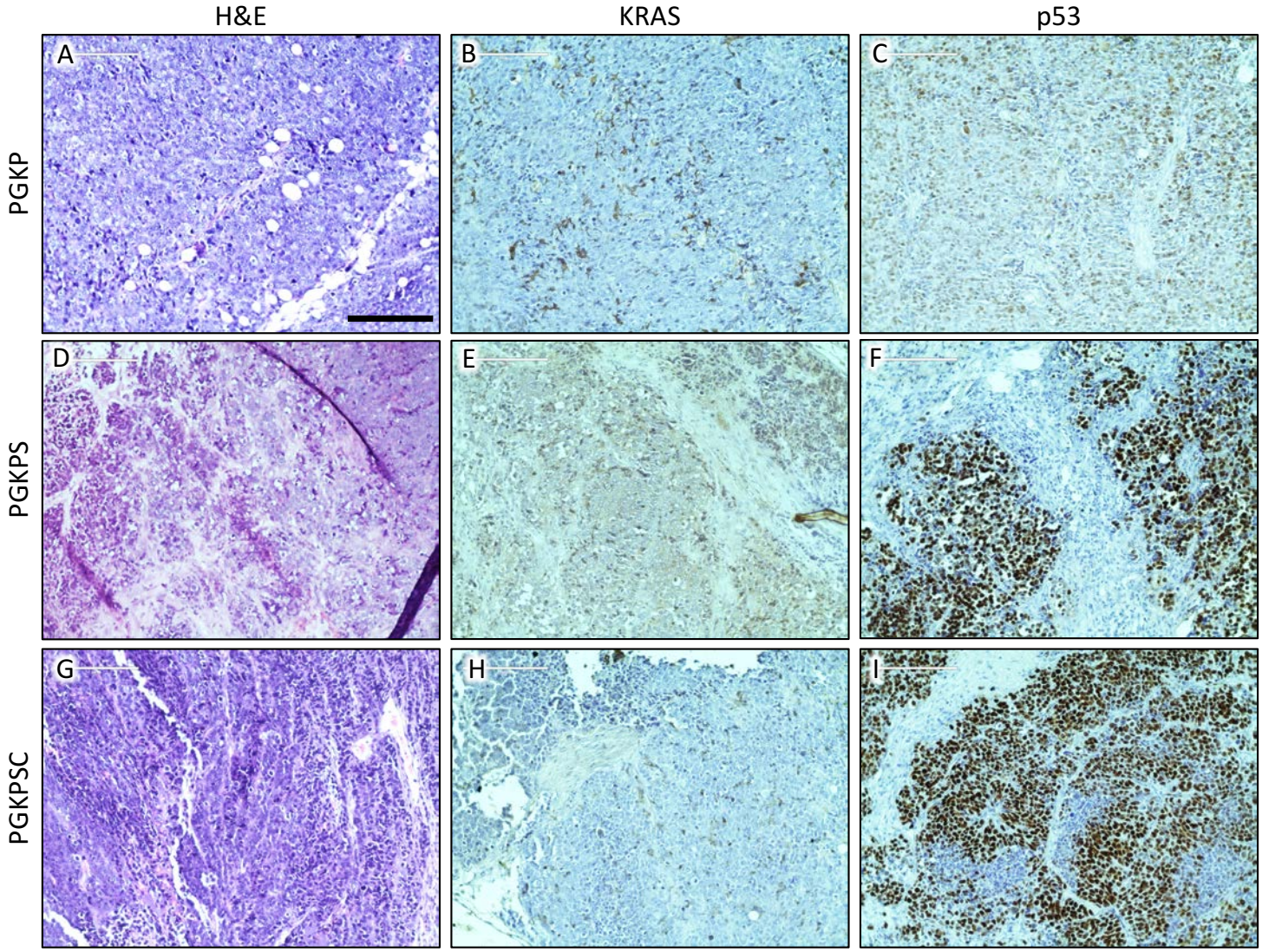

Supplementary Figure 3